

NAVIGATION-GRADE INTERFEROMETRIC FIBER OPTICAL GYROSCOPE

Yu.N. Korkishko^a, V.A. Fedorov^b, V.E. Prilutskii^c, V.G. Ponomarev^d, V.G. Marchuk^e, I.V. Morev^f,
S.M. Kostritskii^g, E.M. Paderin^h

RPC "OPTOLINK" Ltd., Moscow 124498, Zelenograd, proezd 4806, h.5, Russia
Tel. (+7-095) 536-9933, Fax (+7-095) 536-9934, E-mail: opto@optolink.ru

L.P. Nesenjukⁱ, A.S. Buravlev^j, L.G. Lisin^k

*Federal State Unitary Enterprise Central Scientific and Research Institute (CSRI) "ELEKTROPRIBOR" 30, Malaya
Posadskaya str., Saint Petersburg 197046, Russia*
Tel: (+7 812) 232-59-15, Fax: (+7 812) 232-33-76 E-mail: office@eprib.ru

Abstract

Keywords: optical fiber, closed-loop fiber optical gyroscope,

Optolink's navigation-grade (0.01 deg/h) closed-loop interferometric fiber optical gyroscope (FOG) is described. FOG is based on the Sagnac effect, which produces a phase difference $\Delta\Phi_s$ proportional to rotation rate Ω in the ring interferometer. Test results obtained at CSRI "Electroprigor" are presented.

Introduction

Other the last 30 years the interferometric fiber-optic gyroscope (FOG) research and development has evolved from promising experiment to an industrial device used for many applications. FOG is based on the Sagnac effect [1] which states that an optical path length difference is experienced by light beams propagating along opposite directions in a rotating frame. In fiber optical gyroscopes these two counterpropagating waves propagates at closed fiber coil. The obtained phase difference $\Delta\Phi$ is proportional to rotation rate Ω .

We present single-axis FOG SRS-1000 with fiber length 500 m. Size of device is diameter 150x40 mm, weight – 0.8 kg.

FOG configuration

Our 1-axis FOG SRS-100 has minimum configuration (Fig.1) that provides reciprocal optical paths for two beams counter-propagating in a fiber loop. The FOG consists of the one Light Source – Superluminescent Light Emission Diode with central wavelength 1500 nm, one Photodetector, Fiber Splitter (1:1) to divide the light into two parts, ring interferometer to sense angular rate, and printed circuit boards installed signal processing circuits. The ring interferometer consists of a multifunction integrated optic chip (MIOC) and polarization maintaining (PM) fiber coil [2,3]. The MIOC is a three-port optical gyrochip fabricated at lithium niobate wafer by high temperature proton exchange technique [4,5] which provides three functions. First, it polarizes the propagating light to reduce bias instability due to polarization non-reciprocity. Second, it splits the light into clockwise and counterclockwise waves, each with equal optical power and recombines them with a Y-junction waveguide. Third, with electro-optical phase modulator, it applies a biasing phase shift between the counter-propagating beams. PM fiber is used in order to reduce both the drift caused by the polarization cross coupling and the drift caused by earth's and outside magnetic field via the Faraday effect.

^a Doctor of Phys.&Math. Sciences, Professor, General Director

^b Doctor of Phys.&Math. Sciences, Professor, Technical Director

^c Director of Saratov branch

^d PhD in Technical Sciences, Chief Designer

^e Principal Engineer

^f Principal Engineer

^g Doctor of Phys.&Math. Sciences, Head of Section

^h Chief Technologist

ⁱ Doctor of Technical Sciences, Professor, Head of Section

^j Engineer of 1st category

^k Engineer of 2nd category

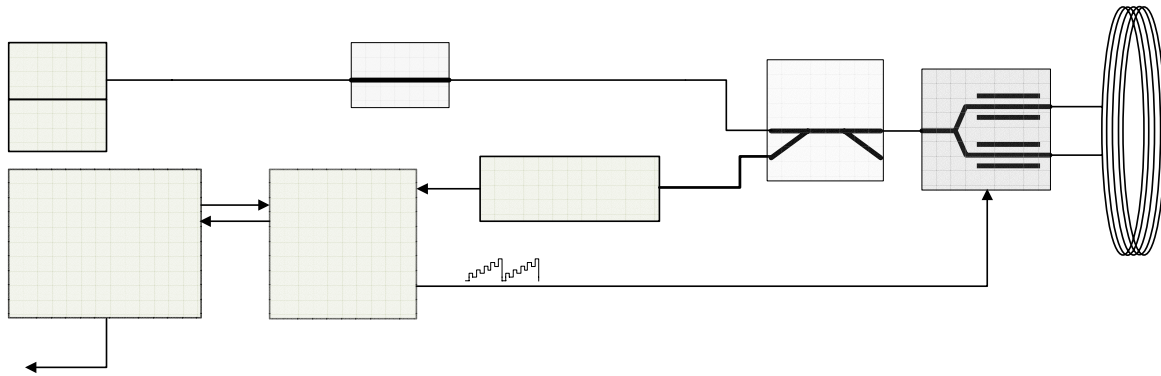


Fig.1. Configuration of FOG SRS-1000

Digital signal processor (DSP) generates voltage for “sawtooth” light modulation for compensation of Sagnac phase shift and to make fixed phase shift $\pi/2$. As a result, each channel is working in closed-loop regime.

Fig.2 shows the scheme of DSP.

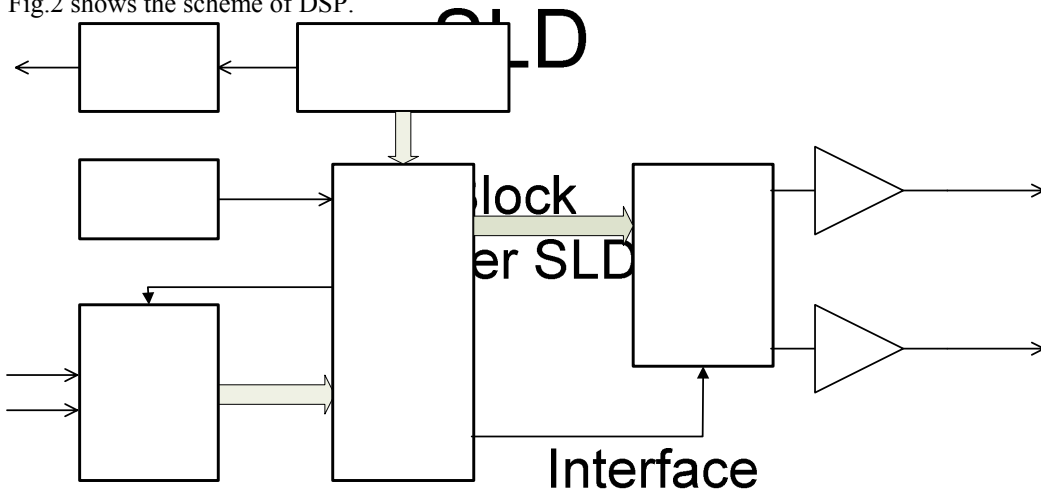


Fig.2. Block diagram of DSP

ADC – analog digital converter, DAC – digital analog converter, FPGA – Field Programmable Gate Array, PD unit – photodetector unit.

Analog signal from analog phase sensitive detector (PSD) that processes the output of the FOG photodetector is amplified and passed to high frequency analog to digital converter (ADC). The digital signal is demodulated by Altera Field Programmable Gate Array (FPGA). Obtained code passed to digital integrator. The code of signal from integrator is using to obtain the slope of phase “saw-tooth” which corresponds to rotation rate. The Digital to Analog converter creates the analog signal as saw-tooth voltage and pass it to MIOC. The wideband integrated optic phase modulators placed at both arms of MIOC are employed to introduce phase ramp modulation, thus enabling close-loop operation. The loop closure scheme uses a digitally synthesized saw-tooth (serrodyne modulation) of 2π amplitude in optical phase shift. In this case the Sagnac phase shift is compensated by saw-tooth modulation of light with calibrated amplitude 2π and frequency f , determined from well-known equation:

$$f = \frac{D}{n\lambda} \Omega$$

where Ω is a rotation rate, D – diameter of fiber coil, n - effective refractive index of waveguiding mode, λ - wavelength.

The frequency of resulting ramp is then a digital measure of the rotation rate, with each ramp reset proportional to the angular turned, i.e. one ramp is equal to $\frac{n\lambda}{D}$. To increase resolution of gyro the rotation rate is determined by measuring slope of phase saw-tooth.

DSP represents the circuit based on Altera's FPGA. DSP is connected with high-speed ADC and with two fast Analog Devices's DAC. Clock pulse for DAC and ADC are drawing up by FPGA. Work of FPGA are clocked by external thermo-stabilized generator.

On one of DSP the Atmel's microcontroller is established which is working as the loader for FPGA. Controller provides an exchange on interface RS-485 with external devices. The monitor for device settings is realized based on this controller. Except for loading FPGA, the controller reads out the data of measurements from FPGA.

Fig.6 shows the functional scheme of the digital automation realized on FPGA.

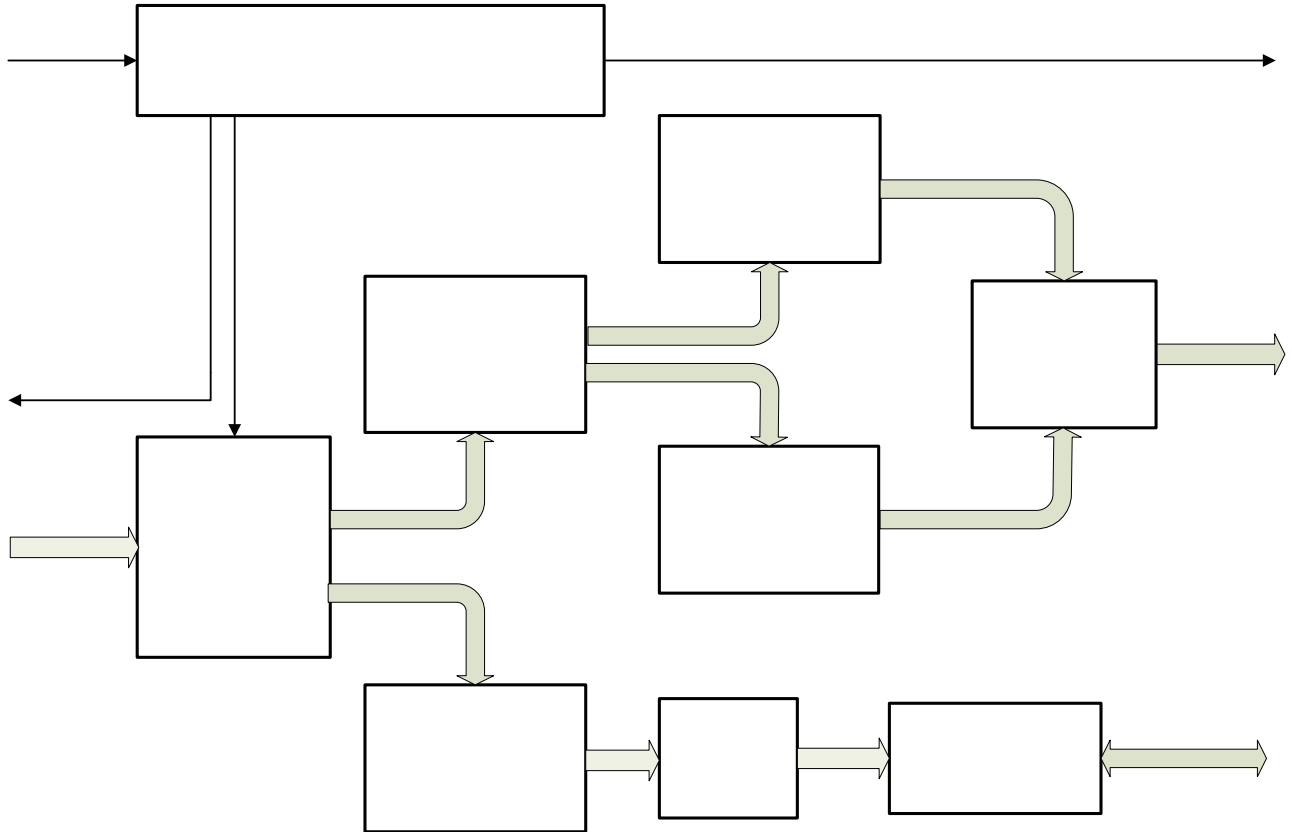


Fig.3. Functional diagram of the digital automation

The shaper of clock pulses transforms clock frequency to a set of impulses for synchronous work management of all devices and units. Clock frequency f_{clk} gets out to multiple frequency f_{am} . Clock pulses for DAC are formed on fronts AM. Clock pulses for ADC are formed so that to exclude measurements on fronts of a signal from PD.

The circuit of processing the signal coming from PD consists of the integration block, the buffer for storage of the measured value and the differencing circuit. The sum of the values of mismatch signal measured on the current phase AM is collected at integration block. On the buffer the sum of the values measured on previous phase AM is stored. After the measurements the values from the integration block and from the buffer pass to the differencing circuit. Depending on current phase of AM, one number passes as deducted and another as the subtractor. Thus the amplitude of a variable signal is allocated taking into account its sign.

The code with sign, corresponding to a sign of a mismatch signal, passes to the digital integrator which consists of the multiplier and the summing unit with the circuit of restriction. The time constant of the digital integrator is setting by the multiplier. The summing unit is used as the integrator. The code from the integrator passes to the shaper of the code for compensating modulation and through the digital filter to the serial interface of connection with the controller.

The shaper of a code for compensating modulation includes the summing unit which forms the "saw-tooth" code and the second summing unit which is used in a contour of a digital regulator of amplitude of compensating modulation. The signal from the circuit of processing of a signal from PD taken off at the moment of recessions of "saw-tooth" serves as signal of a mismatch for a digital regulator of amplitude of compensating modulation. The same signal is used for fine tuning of amplitude of auxiliary modulation.

In SRS-1000 we tried to reduce influence of Fundamental Limitations of FOG performance:

Optical losses

Sensitivity of FOG is limited by shot noise that goes as the square root of the power, that decreases with fiber length. However, the Sagnac effect increases with the length of the fiber. These two competing effects set the length of the fiber for a given sensitivity.

Thermal Noise

Time dependent temperature gradient along the length of the fiber can introduce spurious phase shifts due to the temperature dependence of the refractive index of fiber. To minimize this effect the fibers with smaller dn/dT dependence should be used. Also, quadropole winding such that equidistant points from fiber center are physically close to each other strongly reduce this effect.

Backscattering of light

Backscatter at the output-input couplers and MIOC faces can interfere with the main beams creating parasitic interferometers. Immersion cell to reduce index of refraction step as well as using of tilted MIOC faces reduce backscattering.

Optical Kerr Effect

Electric fields of the counter-propagating beams can cause changes in the index of refraction that is nonreciprocal if light is splitting at unequal parts [6]. The nonreciprocity induced by the nonlinear Kerr effect can be strongly reduced with broad-band, low coherence, unpolarized optical sources or even with a simple 50% duty cycle modulation of the input optical power.

Magneto-optical effect

The magneto-optical Faraday effect is a nonreciprocal effect which is potentially dangerous in adding to the Sagnac effect. This problem is now almost solved by the use of carefully untwisted polarization maintaining fibers as well as by using cases from special materials (permalloy, etc.)

For the IFOG with perfect components (ideal splitter, no backscattering, etc.), the measurement limit is imposed by the shot noise in the light as measured by photodetector [7]. The uncertainty $\delta\Omega_\pi$, generated by the fluctuation in the light due to shot noise can be expressed as [8].

$$\delta\Omega_\pi = \frac{c}{L \cdot D} \frac{\lambda/2}{(n_p n_D \tau)^{1/2}}$$

where n_p is the number of photons per second coming to photodetector, n_D is detector quantum efficiency and τ is averaging time

Experimental results

IFOG SRS-1000 has been characterized at Federal State Unitary Enterprise Central Scientific and Research Institute "ELEKTROPRIBOR" by using rotation table AC1120E (Acutronic) and temperature chamber VT7004 (Voetsch Industrietechnik) [9].

Alan variation was used for calculation of noise characteristics. Dependences of bias drift and scale factor on temperature was obtained by scanning temperature with rate 5°C/h. Scale factor was determined as

$$K = \frac{4\pi}{U_+ - U_-}, \quad \text{where} \quad U_+ = \frac{\sum_{i=1}^n U_{+i}}{n} T - \text{integral of output signal for time T of clockwise rotation,}$$

$$U_- = \frac{\sum_{i=1}^n U_{-i}}{n} T - \text{integral of output signal for time T of counterclockwise rotation,}$$

Bias drift

Bias drift and noise of SRS-1000 were determined at switched off driving motor of rotation table

Sampling frequency was 100 Hz. Specially developed software was used for data recording.

Fig.4 shows SRS-1000 output data.

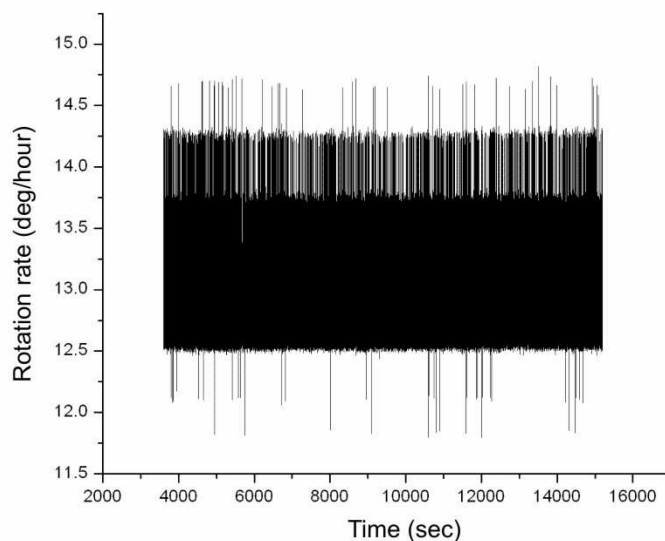


Fig.4. SRS-1000 output data

Smoothed output data obtained by using 1st order filter and time constant 100 seconds is shown at Fig.5.

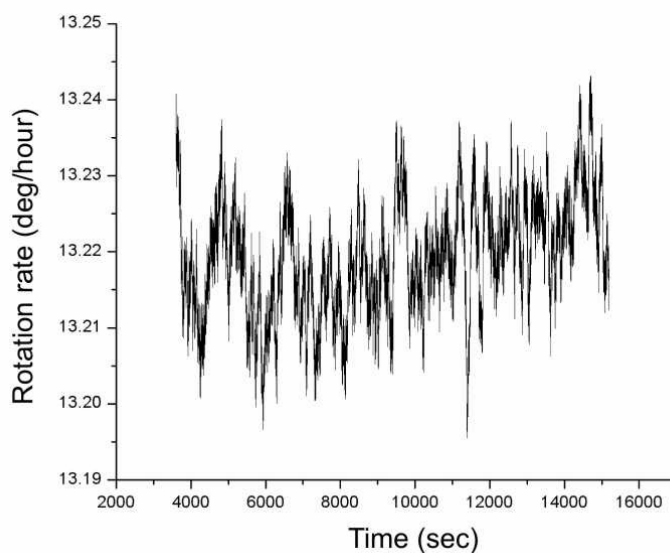


Рис.5. Smoothed rotation rate on time of measurement

RMS of smoothed rotation rate shown at Fig.5 is 0,0075 deg/h.

To determine run to run bias drift we used results obtained from 10 runs. Results are summarized at Table 1..

Табл. 1. Average rotation rate from run to run.

№	Average rotation rate, °/h	RMS, °/h
1.	13.184	0.00797
2.	13.059	0.00698
3.	13.106	0.00693
4.	13.238	0.00735
5.	13.180	0.00669
6.	13.057	0.0082
7.	13.055	0.00852
8.	13.046	0.007
9.	13.049	0.0071
10.	13.044	0.00676
Average RMS		0.00735

From data of Table 2 one can see that bias drift at one run is $0,007 \pm 0,008$ °/h and bias drift from run to run is $0,07185$ °/час. Figs..6 and 7 show uncompensated output and SQRT at different runs.

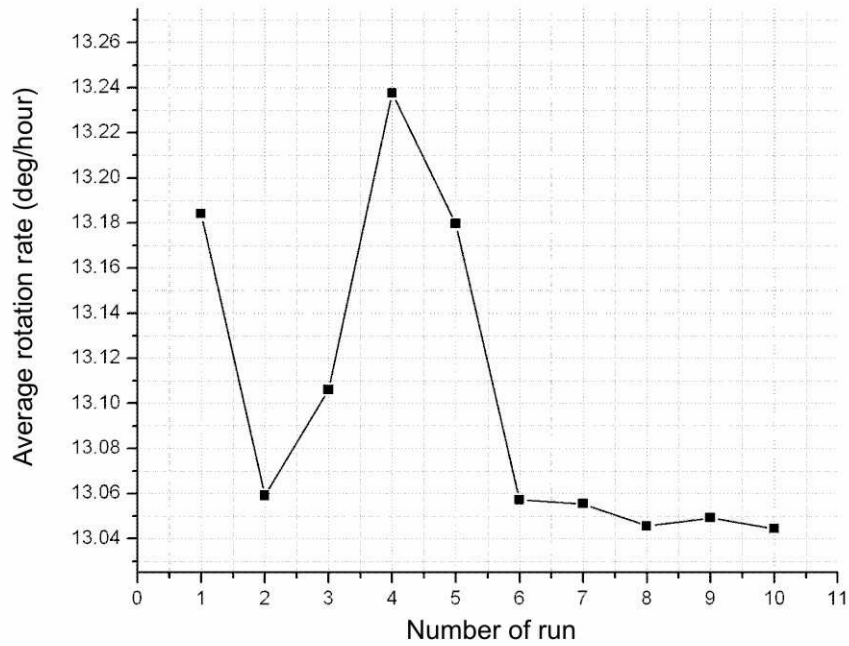


Fig. 6. Average rotation rate from run to run

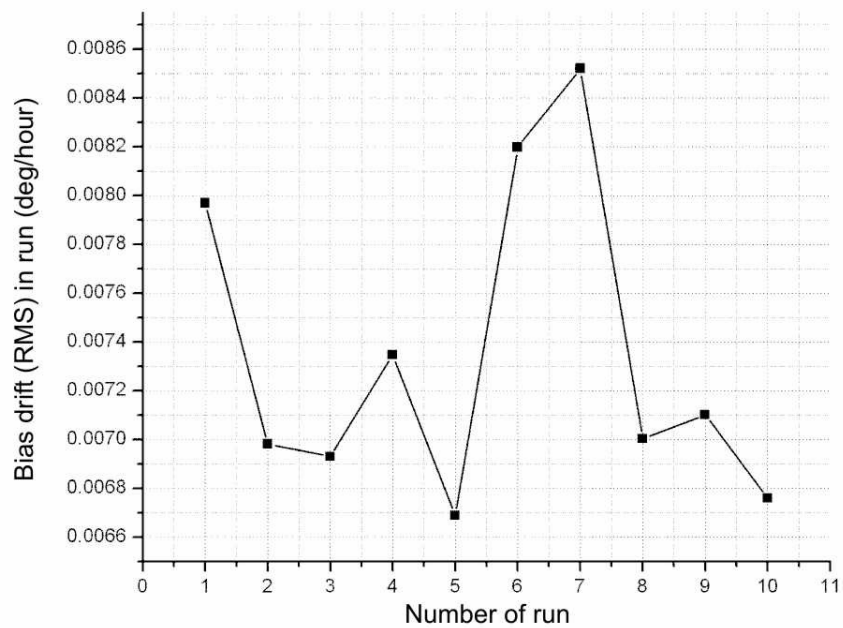


Рис. 7. Bias drift (RMS) from run to run

One can see that average rotation rate variations are less than $\pm 0,01$ °/h. Fig.8 shows output data obtained at different tilted positions. The variations are same as shown at Fig.6. Therefore, one can conclude that bias drift of FOG SRS-1000 is $0,01$ deg/h.

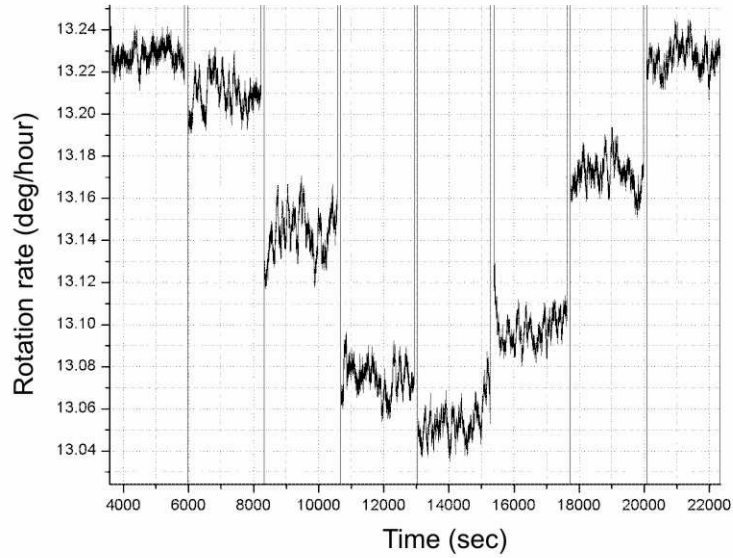


Fig.8. Average rotation rate at different tilted positions.

Fig. 9 shows dependence bias drift on temperature. One can see that bias drift at temperature range from -20°C to $+50^{\circ}\text{C}$ is $\pm 0,15$ deg/h.

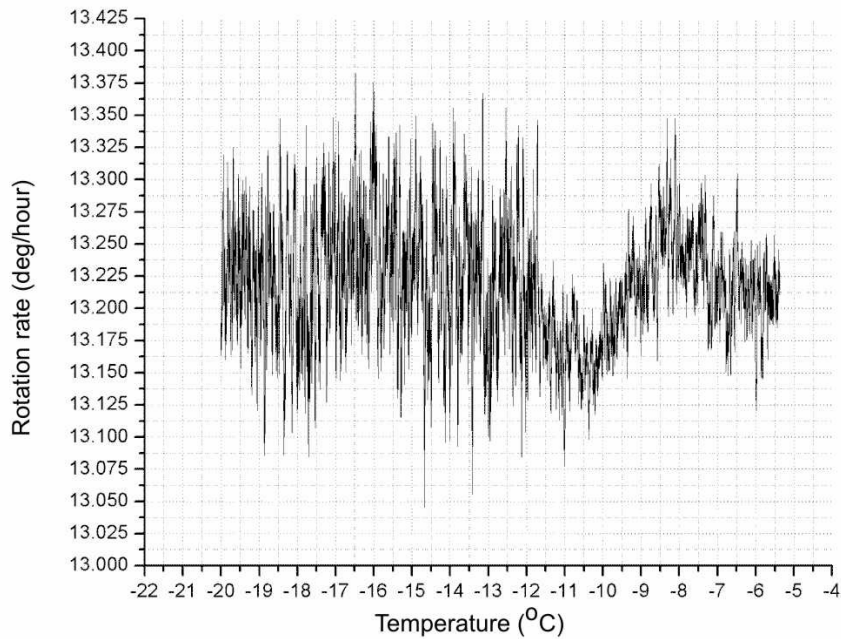


Fig.9. Dependence of bias drift of SRS-1000 on temperature

Scale factor stability

Figs.10 and 11 show scale factor stability of SRS-1000 at constant temperature and in temperature range from -20°C to $+50^{\circ}\text{C}$. One can see that RMS of scale factor at constant temperature is 0.01%. The scale factor stability at temperature range from -20°C to -10°C is $0.0021\ \%/^{\circ}\text{C}$ and at temperature range from $+10^{\circ}\text{C}$ to $+50^{\circ}\text{C}$ is around $6.03 \cdot 10^{-4}\ \%/^{\circ}\text{C}$.

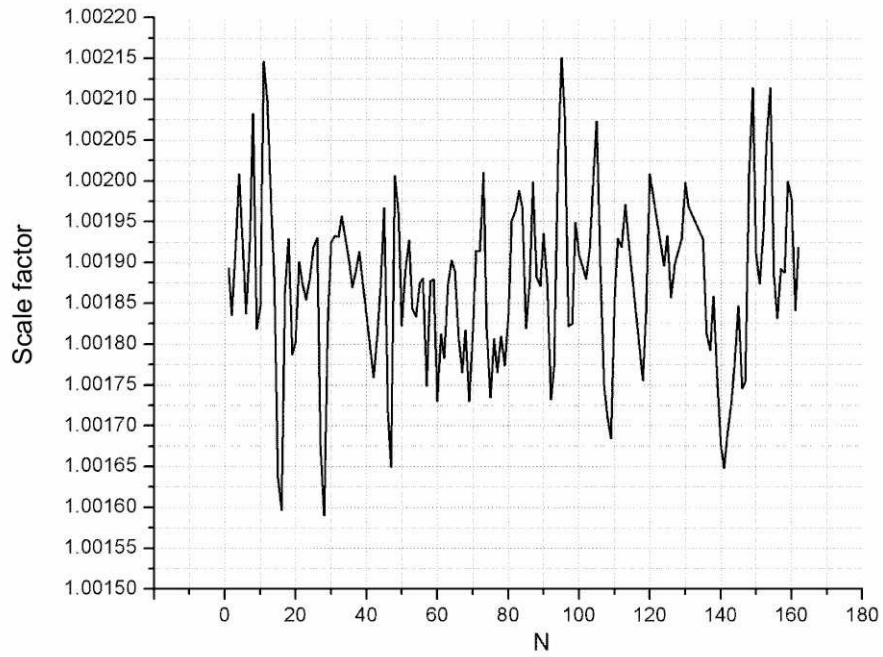


Fig.10. Scale factor vs. number of measuring

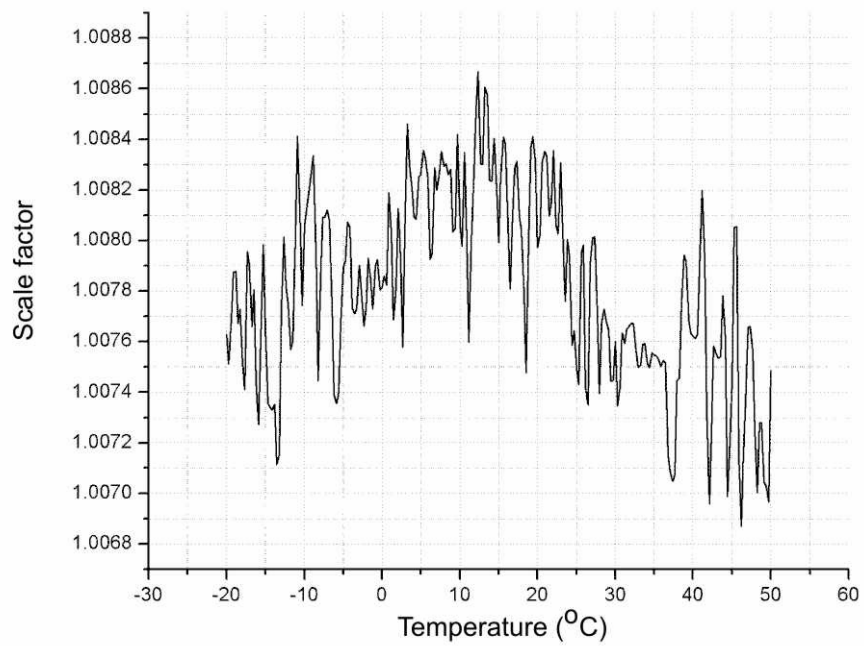


Fig. 11 Scale factor vs. temperature

Scale factor nonlinearity

To determine scale factor nonlinearity of FOG SRS-1000 input rotation rates from -20 to +20 deg/sec with step 1 deg/sec were used. Fig.12 shows deviations of output rotation rates on input rotation rate. Estimated scale factor nonlinearity is 0.001%.

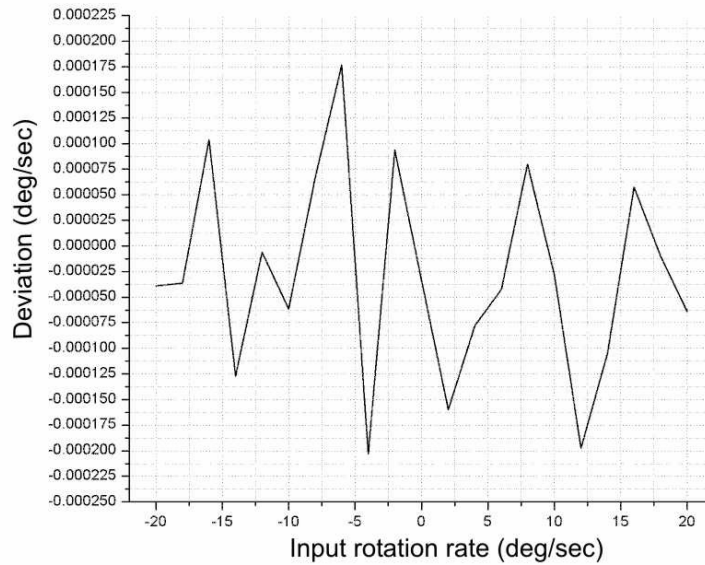


Fig 12. Deviations of output rotation rates on input rotation rate.

Influence of magnetic field

Constant magnetic field parallel to each axis of FOG were applied. Results obtained show that sensitivity of SRS-1000 to magnetic field is following:

- less than 0.05 deg/h/Oe for X-axis (sensitive axis of gyro);
- less than 0.13 deg/h/Oe for Y- and Z- axes placed at FOG plane.

Sensitivity of FOG

Sensitivity of FOG SRS-1000 was measured in the range from $\pm 0,001$ to ± 10 deg/h by changing projection of earth rotation to gyro axis by tilting FOG. Averaging time was 100 sec. One can see that FOG recognizes rotation rate 0.01 deg/h.

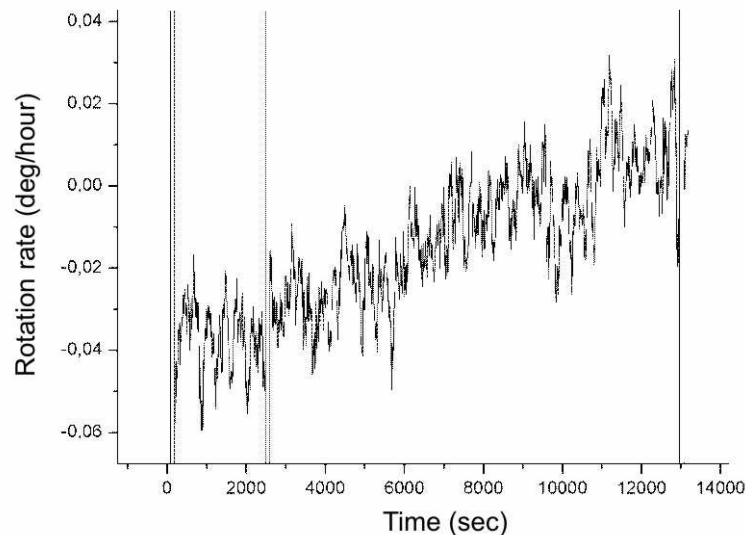


Fig. 13. Output data of SRS-1000 with changing input rotation rate (projection of Earth rotation) from -0.04 to 0,01 °/h)

Results and conclusion

The obtained results are following:

1. At stabilized temperature ($\pm 0,2^{\circ}\text{C}$) the root mean square at one run is $0,007-0,008$ deg/h, and 0.01 deg/h for run to run.
2. Scale factor stability at rotation rate 2 deg/sec is 0.01% ;
3. Scale factor stability did not exceed 0.2% at temperature range from -20°C to $+50^{\circ}\text{C}$;
4. Bias drift at full temperature range from -20°C to $+50^{\circ}\text{C}$ was ± 0.15 deg/h;
5. Scale factor nonlinearity is 0.001 %.
6. FOG sensitivity was not less than 0.01 deg/h

References

1. Lefevre H., The Fiber – Optic Gyroscope, Artech House, 1993.
2. Коркишко Ю.Н., Федоров В.А., Прилуцкий В.Е., Пономарев В.Г., Фенюк М.А., Марчук В.Г., Кострицкий С.М., Падерин Е.М., Высокоточный волоконно-оптический гироскоп с линейным цифровым, // Гироскопия и навигация, 2004. N1 - С.69-82.
3. Прилуцкий В.Е., Пономарев В.Г., Марчук В.Г., Фенюк М.А., Коркишко Ю.Н., Федоров В.А., Кострицкий С.М., Падерин Е.М., Зуев А.И., Интерферометрические волоконно-оптические гироскопы с линейным выходом // Гироскопия и навигация, 2004. N3 - С.62-72.
4. Korkishko Yu.N., Fedorov V.A., Feoktistova O.Y., LiNbO₃ Optical Waveguide Fabrication by High-Temperature Proton Exchange // J. Lightwave Technology, 2000. Vol.18 - P.562-568.
5. Korkishko Yu.N., Fedorov V.A., Kostritskii S.M., Alkaev A.N., Paderin E.M., Maslennikov E.I., Apraksin D.V., Multifunctional integrated optical chip for fiber optical gyroscope fabricated by high temperature proton exchange // in Integrated Optical Devices: Fabrication and Testing, G.C. Righini, Editor, Proc. SPIE, 2003. V.4944 - P.262-267.
6. Frigo N.J., Taylor H.F., Goldberg L., Weller J.F., Rashleigh S.C., Opt.Lett. 1983, V.8 – P.119.
7. Lin S., Giallorenzi T.G. Appl.Optics 1979, V.18 – P.915.
8. Davis J.L., Ezekiel S., 1978, Proc.SPIE, V.157 - P.131.
9. Программа и методика исследования характеристик волоконно-оптических датчиков вращения. Проект ЦНИИ «Электроприбор», 2004.